

## Automatic Detection of Anatomical Landmarks of the Aorta in CTA Images

Pablo G. Tahoces, Daniel Santana-Cedrés,  
Luis Alvarez, Miguel Alemán-Flores,  
Agustín Trujillo, Carmelo Cuenca, and Jose  
M. Carreira

Received: date / Accepted: date

**Abstract** Computed Tomography Angiography (CTA) is one of the most common vascular imaging modalities. However, for clinical use, it still requires laborious manual analysis. This study demonstrates the feasibility of a fully automated technology for the accurate detection and identification of several anatomical reference points (landmarks), commonly used in intravascular imaging. This technology uses two different approaches, specially designed for the detection of aortic root and supra-aortic and visceral branches. In order to adjust the parameters of the developed algorithms, a total of 33 computed tomography scans with different types of pathologies were selected. Furthermore, a total of 30 independently selected computed tomography scans were used to assess their performance. Accuracy was evaluated by comparing the locations of reference points manually marked by human experts with those that were automatically detected. For supra-aortic and visceral branches detection, average values of 91.8% for recall and 98.8% for precision were obtained. For aortic root detection, the average difference between the positions marked by the experts and those detected by the computer was  $5.7 \pm 7.3$  mm. Finally, diameters and lengths of the aorta were measured at different locations related to the extracted landmarks. Those measurements agreed with the values reported by the literature.

**Keywords** Computed Tomography (CT) · Aortic Root · Aortic Branches · Detection · Vessel Morphology

---

Pablo G. Tahoces  
DEC, Universidad de Santiago de Compostela, Santiago de Compostela, Spain  
E-mail: pablo.tahoces@usc.es

Daniel Santana-Cedrés, Luis Alvarez, Miguel Alemán-Flores, Agustín Trujillo, and Carmelo Cuenca  
CTIM, DIS, Universidad de Las Palmas de Gran Canaria, Las Palmas de Gran Canaria, Spain

Jose M. Carreira  
Complejo Hospitalario Universitario de Santiago (CHUS), Santiago de Compostela, Spain

## 1 Introduction

Morphological characteristics of the vasculature have been traditionally analyzed for the diagnosis of certain pathologies [9], as well as for follow-up and planning of endovascular surgery and other interventions [24]. Moreover, it has been demonstrated that an independent measure of cardiovascular risk can be associated with arterial stiffness [22, 18].

Computed Tomography Angiography (CTA) is a well established imaging modality for providing anatomical information about diseases related with the morphology of several structures. The arrival of the multidetector row CT (MDCT), provides isotropic 3D images, from which accurate and reliable information like diameter lengths, volumes and other shape parameters can be extracted [11]. Based on this information, several clinical guidelines have been published [4, 13]. Thereby, some quantifiable imaging characteristics for the evaluation of normality or severity, degree of change, or the state of a disease, injury, or chronic condition in relation to normality are now available [1].

The analysis of the morphological features of the vasculature related with its diameter and/or its shape can be improved by means of the introduction of computer tools that can provide more accurate and reproducible values for such biomarkers. However, the development of these computer tools requires a standardized way of representing the information, in order to afford a good reference for modeling the vascular tree in terms of a vessel graph [19].

Anatomical labeling of the vasculature is not always a trivial task, as its topology may change from patient to patient. In most cases, manual procedures have been applied for establishing the different levels where the morphological aortic measurements have to be extracted. This is the case for Turkbey *et al.* [29] who take the axial plane at the level of the right pulmonary artery as a reference to determine the normal size of the diameter of the ascending aorta and its relationship to age, gender or race/ethnicity. Cleemann *et al.* [6] determine the diameter of the thoracic aorta in nine positions related with anatomical landmarks of the aorta. Entezari *et al.* [10] evaluate thoracic aortic aneurysms by analyzing the aortic diameter at seven selected points related with anatomical landmarks. Redheuil *et al.* [25] have analyzed the relationship between the geometric changes of the aortic arch and the age of the patient. Length, diameter and curvature of the aortic arch were analyzed for this task. Finally, Sugawara *et al.* [27] have studied the relationship between human aorta lengthening and aging. In general, we can conclude that there is a limited number of anatomical landmarks that have been typically employed as references for the extraction of morphological information in the aorta.

While most of the published studies make use of manual procedures to place these landmarks, several attempts have been carried out to develop algorithms that automatically perform this task. In this sense, Elatar *et al.* [8] proposed an algorithm for detecting the sinotubular junction and the two coronary ostia in CTA volumes. Queiros *et al.* [23] proposed a semi-automatic method to extract measurements at four relevant anatomical levels: left ventricular outflow tract (LVOT), aortic annulus, sinus of Valsalva, and sinotubular junction, for electrocardiography datasets. Kitasaka *et al.* [16] presented a method for automatic labeling of upper abdominal arteries using branching information. Oda *et al.* [21] presented

a knowledge-based framework for anatomical labeling of bronchial branches and major abdominal arteries associated with the colon.

The main contribution of this paper is the development of a new method for the extraction and labeling of several standard landmarks, related to the geometry of the aorta from CTA volumes. In this way, both the aortic root and its main branches can be detected and tagged automatically. To adjust the parameters used in the development of the proposed algorithms and to test the results obtained, two independent data sets were used. Performance was evaluated by comparing the positions calculated by the method with those established by human experts. Finally, diameters and lengths of the aorta at different locations were calculated and compared with those published in the literature to determine the validity of the results obtained.

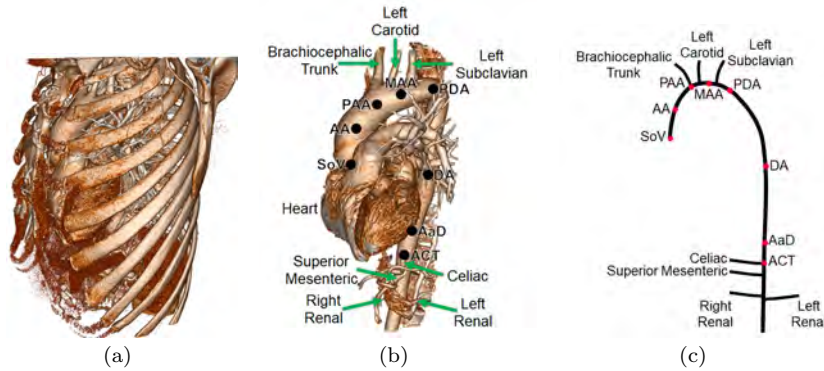


**Fig. 1** Vascular tree of the aorta with the main branches and location of the landmarks: (a) full CT volume, (b) details of the chest vasculature, and (c) schematic representation. Tags are included for: sinus of Valsalva (SoV), mid ascending aorta (AA), proximal aortic arch (PAA), mid aortic arch (MAA), proximal descending aorta (PDA), mid descending aorta (DA), aorta at the aortic hiatus of diaphragm (AaD), and aorta at the level of the celiac trunk (ACT). Renderized 3D volumes were obtained by means of the *3DSlicer* software package [15]

## 2 Methods

As explained above, the aim of this study is to automatically extract and label several anatomic landmarks to perform standard measurements related with the diagnosis and the evolution of the shape and size of the aorta. In this sense, we have selected eight of the nine landmarks defined by Hiratzka *et al.* [13] (red dots of Fig. 1). Namely, SoV, AA, PAA, MAA, PDA, DA, AaD, and ACT. Furthermore, some other lateral branches, like the superior mesenteric or even both renal arteries were also located in those cases in which they appear as part of the CT volume. Detection of the Sinotubular Junction was discarded in this paper due to its proximity to the sinus of Valsalva. Moreover, the cases we use were not acquired with ECG-gated cardiac MDCT (it was not the purpose of this study) and this implies the presence of movement artifacts, especially in the root of the aorta, that make the detection of this landmark quite challenging.

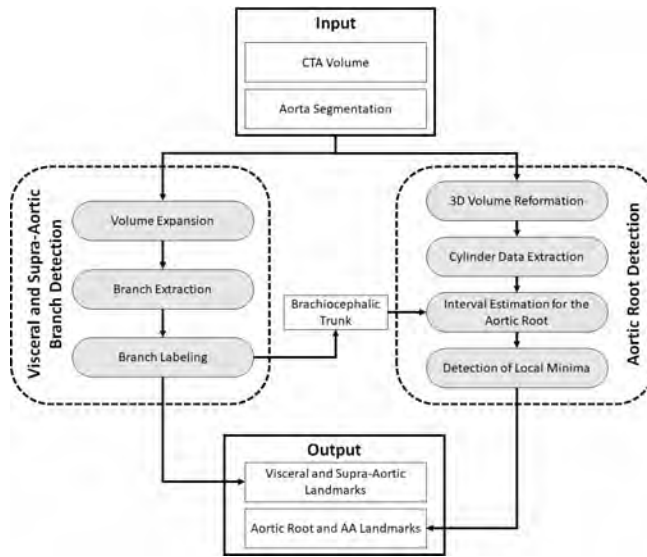


**Fig. 2** General flowchart to extract landmarks from CTA volumes.

We emphasize that some of these landmarks were not directly achieved, since they require additional calculations or even the detection of some additional points. This way, the problem to solve requires two different phases. A first step, where the extraction and identification of the main branches of the aorta and the aortic root is the main target. A second step, where the locations of the landmarks that were not directly obtained can be derived from the locations extracted in the first step.

Figure 2 illustrates the pipeline of the proposed scheme. The procedure starts with a set of axial slices that conform a CTA Volume. A segmentation procedure is then performed. As a result the lumen of the aorta, its centerline, a cross-section for each point on the centerline (on the plane orthogonal to the centerline), and a probability distribution of the intensities inside and around the lumen are extracted. In our case all this information is provided after applying the methods described in [28] and [2]. Then, two sub-processes, one dedicated to the extraction of the supra-aortic and visceral branches, and another for the detection of the aortic root, are implemented. Finally, the estimation of the location of the landmarks not directly extracted from the above stages is performed.

## 2.1 Visceral and Supra-Aortic Branch Detection

Visceral and supra-aortic branches connect to the aorta at different locations along its path. The same iodinated blood that travels through the aorta fills those structures and no significant changes in the intensity can be appreciated when comparing the lumen of the aorta with those of the branches. Therefore, the branches represent leakage points where region growing algorithms can evolve from the aorta. Nevertheless, we are interested in the main branches and the non-relevant

ones, as well as other possible expansion regions which do not correspond to the branches, have to be removed.

Aiming to clarify the description of the algorithm, we include a flowchart with the main stages in Fig. 3: the initial volume, its expansion, the automatic branch extraction, and the branch labeling, which are explained below.

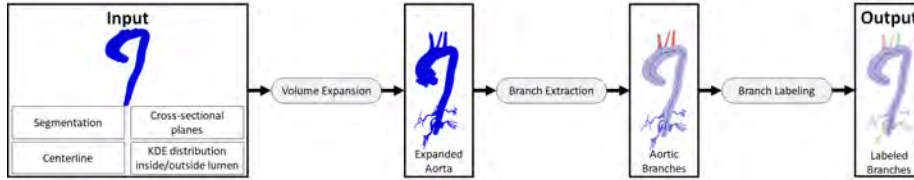


**Fig. 3** Flowchart of the algorithm to extract the visceral and supra-aortic branches.

### *Volume Expansion*

The initial information provided by the method in [2] consists of a 3D volume with the main artery, i.e. the aorta solely, the centerline of the vessel, the cross-sectional planes and the probability density distributions of the intensities inside and around the aorta [3]. This information can be attained by using any segmentation technique. Nevertheless, the use of the method described in [2] has the advantage of providing all of them automatically, without requiring further computations. Starting from the 3D volume, an expansion process is carried out in order to make the vessel grow towards regions with similar intensities (i.e. through leakage points). These are regions where the intensity corresponds to those of the blood, according to the probability density distributions provided as initial data. In most cases, we can assume that those leakage points correspond to the junctions of the aorta with its branches or perhaps with the heart. However, in some regions the expansion may not correspond to real ramifications (e.g. the heart, which is not within our objectives) and, for this reason, the process is performed in two phases. First, the probability of the distribution of the intensity inside/outside the aortic lumen is used and, with the aim of identifying possible wrong expansions, we sprawl the aorta up to a limited distance (a threshold of 20 mm has been experimentally set) from its original segmentation. In case the added volume achieved in this step is too large, it is labeled as “wrong ramification” (i.e. the heart, as shown in Fig. 4(b) with red voxels). If the added volume is too small, it is discarded because it corresponds to isolated groups of voxels. In the second phase, we repeat the expansion with a higher limit for the distance, but avoiding the regions tagged as “wrong ramification”. This way, the volume expands towards areas with similar intensities to those of the aorta which grow gradually (Fig. 4(c)).

### *Branch Extraction*

From the previous step, we obtain an expanded version of the volume, including the aortic branches. If we compute the difference between the new volume obtained through the expansion process (Fig. 4(c)) and the initial one (Fig. 4(a)) we obtain

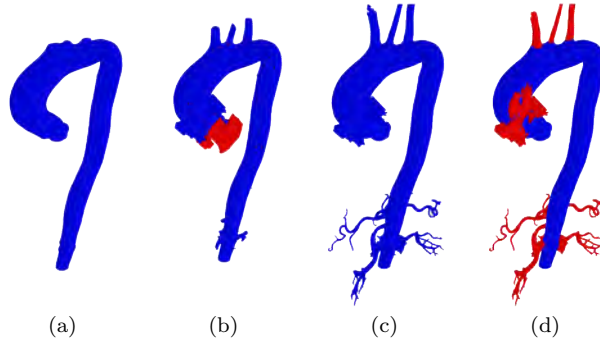


**Fig. 4** Stages to obtain the aorta ramifications: (a) initial segmentation of the aorta, (b) first expansion with the “wrong ramifications” in red, (c) second expansion, and (d) obtained ramifications and aorta in different colors.

the ramifications we are searching for (in red in Fig. 4(d)). Using these two volumes, we can gather some more information, such as the contact zones between them. In this way, those voxels inside the branches which are neighbors of voxels inside the aorta are considered contact areas, because they determine the boundary between the ramifications and the aorta. Figure 5(a) illustrates a section of the aortic arch (blue), the supra-aortic branches (red) and the contact areas (green). Within each contact area, the voxel which maximizes the distance to the edge of the ramification is chosen as the contact point (Fig. 5(b) and 5(c)). That point, is the closest point to the center of the branch.

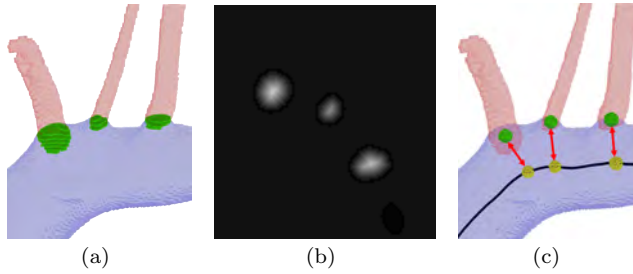


**Fig. 5** Detail of the stages to obtain the contact points: (a) aorta surface and ramifications with the contact regions highlighted in green, (b) detail of a slice of the distance image, and (c) obtained contact points (green) and their closest points (yellow) on the centerline of the aorta.

Afterward, for each of these contact points, we determine what is the closest point on the centerline of the aorta (endpoint) and we can consider it as the representative of the branch within the centerline for further computations. (Fig. 5(c)).

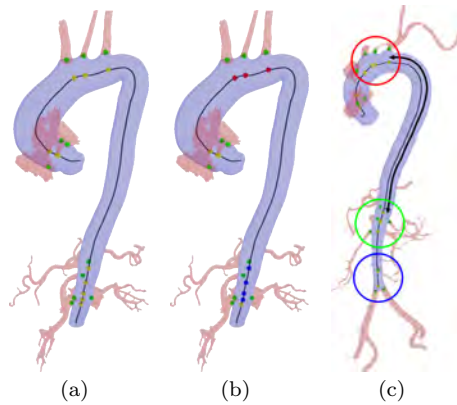


**Fig. 6** Extraction of different groups according to the endpoints of the branches: (a) ■ closest points on the centerline, (b) groups by proximity (■ supra-aortic vessels, ■ visceral vessels), and (c) case with multiple groups of ramifications depicted with circles (○ supra-aortic group, ○ initial (wrong) visceral group, ○ final (right) visceral group, and arrow in ■ which indicates the distance between subclavian and celiac arteries).

### Branch Labeling

After extracting the candidate branches, it is necessary to remove those considered to be false and label the remaining as one of the three supra-aortic or as one of the four main visceral branches of the abdominal region. To perform this task, using a proximity criterion we group the endpoints of the branches, in the aortic centerline (Fig. 6). For each group, we calculate their relative placement, in terms of the patient's anatomy. Thus, the most proximal group (closest to the patient's head) is considered to contain the supra-aortic vessels (red circle in Fig. 6(c)), and the most distal group (closest to the patient's feet) will contain the visceral arteries (blue circle in Fig. 6(c)).

Nevertheless, although the identification of the supra-aortic group is usually clear, in some cases, spurious groups may appear, which could be confused with the visceral group. To prevent this from generating a false identification, we add two conditions to the selection criteria: i) The distance from the left subclavian artery to the distal group must be large enough (a threshold has been experimentally set), and ii) the candidate group with the highest number of branches is more likely to be right one (black arrow and green circle respectively in Fig. 6(c)).

Within the supra-aortic group, we are interested in three vessels. In case we have extracted more than three, we first eliminate those with a small diameter. We also exclude those whose orientation does not correspond to the upper direction in the sagittal plane (Fig. 7(a) left). This orientation is estimated by means of the vector which connects the endpoint on the centerline with the contact point. From the remaining vessels, the closest to the heart is labeled as the brachiocephalic artery. If there are two more branches, the nearest to the heart (excluding the brachiocephalic trunk) is labeled as the left common carotid artery, and the last one as the left subclavian artery. In case only two vessel are remaining, (bovine

arch case) only two branches are labeled: brachiocephalic artery (sharing a common origin with the left common carotid artery) and the left subclavian artery.

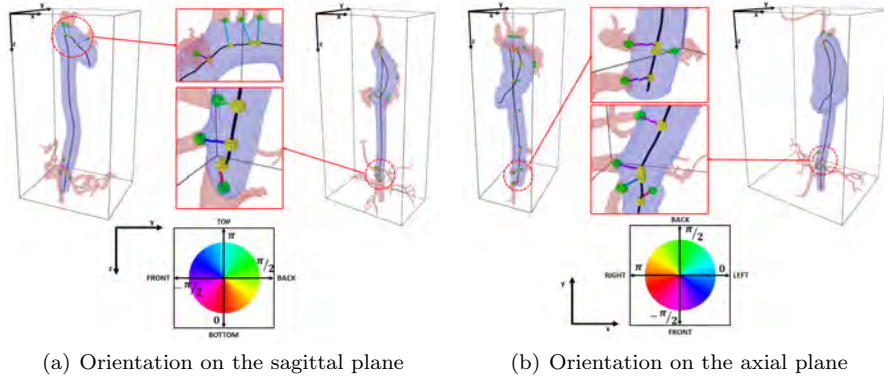


**Fig. 7** Analysis of the orientations for different cases: (a) orientations on the YZ plane for the supra-aortic vessels used to remove branches without upward orientation (left) and for visceral vessels to remove branches with downward orientation (right). In (b) orientations on the XY plane for the visceral vessels to remove branches toward the back (left) and to classify them (right). Both diagrams include zooms in the regions of interest and a color wheel to depict the vector orientation.

Inside the visceral group, we use the orientation as the exclusion criteria. Those arteries which grow towards the feet (Fig. 7(a) right) or towards the back of the patient (Fig. 7(b) left) are removed. Moreover, if the diameter is too small (thin vessels) or the volume associated to the ramification is too large (the branch has touched a different organ with similar intensity and has expanded inside it), the vessel is also excluded. Within this group, the closest vessel to the heart is labeled as celiac artery. Next, the orientation in the axial projection is employed to label the superior mesenteric artery (close to the celiac and similar orientation) and both renal arteries (Fig. 7(b)). For the left renal the orientation must be close to  $0$ , whereas for the right renal, it should be close to  $\pi$  (Fig. 7(b) right, with vectors in blue and red respectively). In Fig. 8 a result of the classification process is shown.

## 2.2 Aortic Root Detection

In a CT volume acquired after iodine contrast has been injected, the lumen of the aorta appears as a radiolucent region. Furthermore, when we focus on that lumen in terms of the gray level of the pixels, almost no changes can be observed between consecutive slices. Now, if we straighten the aorta along its centerline and analyze its lumen, we can conclude that its shape and texture barely change. In the absence of artifacts, the round shape and the radiolucent and homogeneous texture are the basic features observed until the sinus of Valsalva are reached (Figure 9).

One of the possibilities for analyzing that lumen is the extraction of a cylinder of data, located along the centerline of the aorta. In the absence of artifacts, the

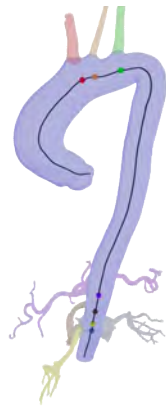


**Fig. 8** Classified branches and their associated points on the centerline: ■ brachiocephalic trunk, ■ carotid, ■ subclavian, ■ celiac, ■ superior mesenteric, ■ left renal, and ■ right renal.

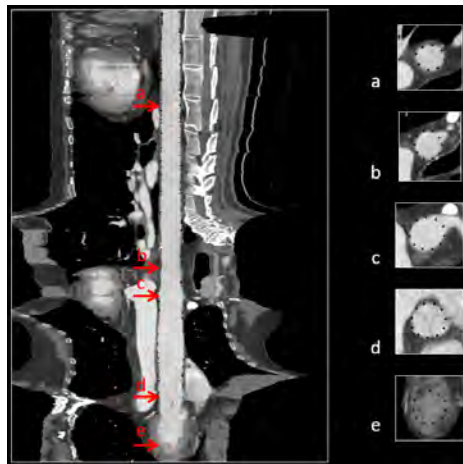


**Fig. 9** The aorta straightened along its central line after reformatting the volume. The figure includes cross-sectional views of the lumen at different places: a) normal lumen, b) left subclavian artery, c) brachiocephalic trunk, d) sinus of Valsalva, e) left ventricle. The black crosses around the lumen of the aorta represent the elliptical estimation of the lumen after applying the segmentation process.

locations in which sharp changes appear are likely to be an interface between the aorta and any other different anatomical structure. Thereby, these regions are good candidates to be aortic root, because this anatomical landmark plays the role of interface between the aorta and the heart.

### *3D Volume Reformation*

The first step for obtaining a cylinder of data that represents the aortic lumen is to build a reformatted version of the CT volume, where the aorta appears straightened. Curved Planar Reformation (CPR) is a way of generating longitudinal cross

sections at each central point of tubular structures such as the aorta in order to show its lumen, wall and surrounding tissues [14]. In our case, this can be done directly by stacking all cross-sectional planes (obtained from the segmentation process) aligned with respect to the centerline of the aorta.

### *Cylinder Data Extraction*

To extract the cylinder of data, reference values of the published aortic diameter were taken into account (see ref. [20]). Thus, a cylindrical mask of radius 1 cm, centered around the centerline of the aorta, is built. The height of this cylindrical mask is half the length of the straightened aorta, for each case (black rectangle inside the aorta in Figure 10(a)). In this way, the voxels within this mask will be taken as representative samples of the central section of the aortic lumen. To perform the analysis, a 1D signal is constructed from this cylinder of data. To eliminate possible artifacts, for each point of the axis of that cylinder, cylindrical segments of height  $CS = 2 * w + 1$  ( $w = 5$  cross-sections, in our case) are taken (Fig. 10(b)). Then, the average of each cylindrical segment is taken as the value of the corresponding cylindrical section at each point i.e. as the value of each point in the constructed 1D signal.

Fig. 10(b) depicts with a continuous line an example of the 1D signal generated ( $avg(z)$ ). In general, the first third of  $avg(z)$  is almost flat or monotonically increasing (labeled as “flat section”). We call  $aValue$  to the average value of the signal in such a region, and  $stValue$  its standard deviation. Furthermore, we observe a clear decrease of  $avg(z)$  in areas close to the aortic root. In order to ease the study, a new signal ( $avgGrad(z)$ ) is generated by applying a gradient filter to  $avg(z)$ . In this new signal, it is easier to analyze the presence of the aortic root, since it has a zero-crossing with a positive slope at each local minimum of  $avg(z)$  (dotted line in Fig. 10(b)). Using the same approach as before, we denote as  $aGradValue$  the average of the signal  $avgGrad(z)$  in the flat section, and  $stGradValue$  its standard deviation. In absence of artifacts, those values are close to zero.

Therefore, it seems that the implementation of an algorithm based on the detection of local minima in a one-dimensional signal should be a possible solution for the detection of the aortic root in reformatted CT volumes like these.

### *Interval Estimation for the Aortic Root*

The detection of local minima can be distorted by the presence of different types of artifacts. To solve this problem, we propose to build a statistical model that restricts the search of any local minimum to a narrow interval of the one-dimensional signal  $avg(z)$ . To build that model, we have analyzed the possibility of linking the location of the aortic root ( $AR$ ) to different anatomical reference points that are usually present in this type of images. We have concluded that the brachiocephalic trunk ( $BT$ ) is a good candidate to solve this problem.

To reach this conclusion, we have manually marked both the location of the  $AR$  and the location of the  $BT$  over the reformatted CT scans that belong to our training set (see Section 2.4). The correlation between the location of  $AR$  and the location of  $BT$  is quite high ( $R^2 = 0.965$ ), and can be visually noticed if we plot  $AR$  against  $BT$  (Fig. 11). Thus, we have concluded that the  $BT$  seems to be

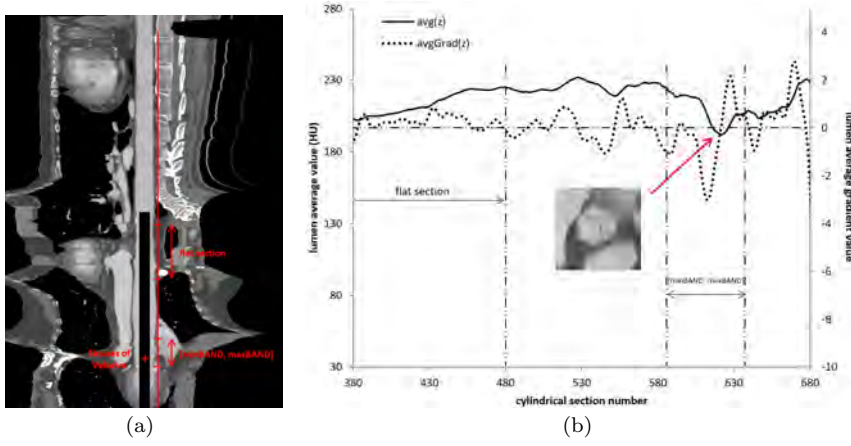


**Fig. 10** Unidimensional representation of  $avg(z)$  and  $avgGrad(z)$ : (a) Straightened aorta with the cylindrical mask superimposed, and (b) plot of the generated 1D signal. The zero of the cylindrical sections is at the bottom of the straightened aorta (top of Fig. 10(a)), while the lumen average value is represented in terms of Hounsfield Units (HU).

The red arrow within the graph indicates the location of the sinus of Valsalva.

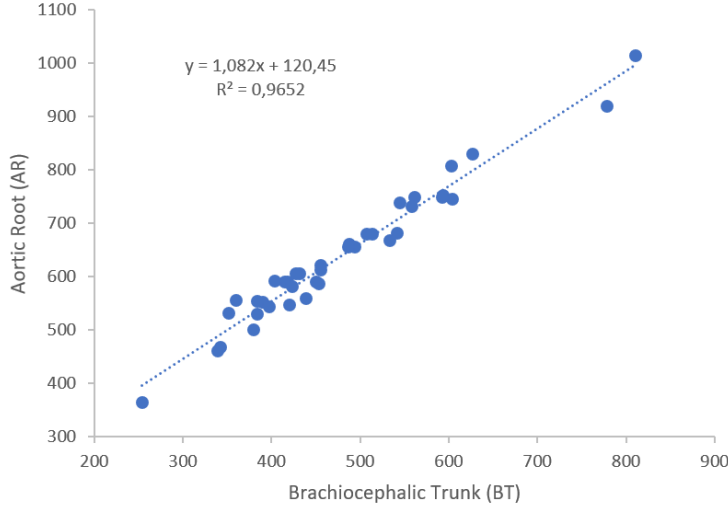


**Fig. 11** Correlation along the centerline of the locations of the Brachiocephalic Trunk and the Aortic Root. The values represented on both axes are in terms of the cylindrical section number (see Fig. 10(b)).

a good reference for the establishment of the theoretical limits of the searching interval over the one-dimensional signal  $avg(z)$ .

Hence, the estimated position of the aortic root for a case  $i$  ( $\widehat{ARp}_i$ ) can be calculated from the BT position of the case  $i$  ( $BTp_i$ ), as follows:

$$\widehat{ARp}_i = \hat{A}_1 BTp_i + \hat{A}_0, \quad (1)$$

where  $\hat{A}_1$  and  $\hat{A}_0$  are the estimated parameters of the linear model adjusted.

The subsequent analysis of the residuals (Q-Q plot analysis)

$$\epsilon_i = ARP_i - \widehat{ARP}_i, \quad (2)$$

demonstrates that those residuals ( $e_i$ ) follow a normal distribution with a mean value  $\mu = 0$  and a standard deviation  $\sigma$ , i.e.:

$$\frac{\epsilon_i}{\sigma} \sim N(0, 1). \quad (3)$$

Thereby, to guarantee that at least 95% of the cases were within the interval, we define the limits of the searching interval  $[minBAND, maxBAND]$  as follows:

$$minBAND = \widehat{ARp}_i - 2\sigma \quad (4)$$

$$maxBAND = \widehat{ARp}_i + 2\sigma \quad (5)$$

#### *Detection of Local Minima*

Detection of local minima in  $avg(z)$  was performed by analyzing the locations of the zero crossings in the  $avgGrad(z)$  signal. In this way, given  $avgGrad(z)$ , each zero crossing where the signal has a positive slope potentially represents a local minimum of  $avg(z)$ .

Hence,  $z_c$  will be a possible candidate to be an aortic root location, if:

$$avgGrad(z_c - 1) < 0 \quad \text{and} \quad avgGrad(z_c + 1) > 0 \quad (6)$$

Among these candidates, a selection is made by restricting the search according to the following criteria:

- i)  $z_c$  has to be located in a bounded interval

$$z_c \in [minBAND, maxBAND] \quad (7)$$

- ii) Spurious local minima of  $avg(z)$  have to be eliminated, i.e the depth of the local minima has to have some entity, which depends on each particular case through  $stGradValue$ :

$$avgGrad(z_c + CS) - avgGrad(z_c) > 3 * stGradValue, \quad (8)$$

where  $CS$  was defined above.

- iii) Artifacts have to be removed:

$$aValue - avg(z_c) > 2 * stValue \quad (9)$$

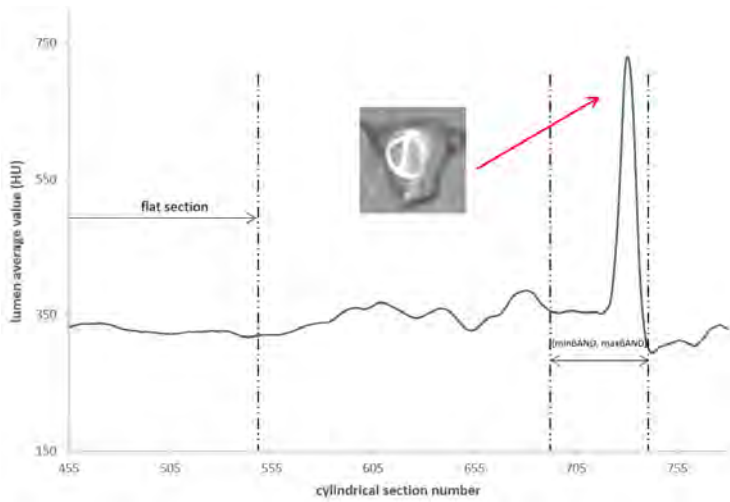


**Fig. 12** Plot of  $avg(z)$  when a TAVI is performed in the aortic root. Like in Fig. 10(b), the zero of the cylindrical sections is at the bottom of the straightened aorta. The red arrow within the graph indicates the prominent positive peak generated by the presence of the valve.

The list of remaining candidates, will represent locations where the original signal  $avg$  has a local minimum of certain entity within the interval  $[minBAND, maxBAND]$ . All of them are susceptible to be the aortic root. To select one of them, the candidates are ordered, according to their  $z$  value and, finally, the candidate with the lowest cylindrical section number is chosen as the root of the aorta.

That is, let  $\{z_{c1}, z_{c2}, \dots, z_{ck}\}$  be the set of remaining candidates. We select as the aortic root the

$$\begin{aligned} z_{ci} &\in [minBAND, maxBAND]_r \mid \forall z_{cj} \\ &\in [minBAND, maxBAND]_r : z_{ci} \leq z_{cj}, j = 1, 2, \dots, k \end{aligned} \quad (10)$$

### Special Cases

If the aortic valve has been replaced by an artificial device (*TAVI, Transcatheter Aortic Valve Implantation*), the pattern of  $avg(z)$  differs from that shown in the normal scenario described above. As a result, there is a prominent positive peak in the  $avg(z)$  profile (Fig. 12). Thus, to include this type of cases, prior to the method described above, an analysis of  $avg(z)$  is performed and, if a significant positive value is found, the position of this peak is assigned as the location of the aortic root.

## 2.3 Estimation of the Location of the Landmarks

Once the different branches and the aortic root have been identified, the landmarks are computed by using the points on the centerline corresponding to them. Namely, the *SoV* is given by the aortic root and can therefore be located directly from the method described in Section 2.2. The *PAA* and the Aorta *ACT* are provided by the

location of both, the endpoints of the *Brachiocephalic Trunk* and the *Celiac Artery*, extracted from the method described in Section 2.1. The remaining landmarks are not directly provided, but can be computed from the endpoints of the branches already detected, following the definitions established at the beginning of Section 2.

#### 2.4 Data Selection and Experimental Setup

63 CT scans provided by the Complejo Hospitalario Universitario de Santiago de Compostela, routinely acquired during clinical practice were employed for the purpose of adjusting, optimizing and testing our method. The only selection criterion was that the thickness of the slice should be less than 1 mm and that both the aortic root and the supra-aortic arteries were visible. We have to remark that most of the patients selected for this study were affected by several aortic diseases, among which aortic aneurysm is the dominant pathology. No Electrocardiography (ECG)-Gated CT scans were included in the study but iodinated contrast medium was administered to all the patients before the acquisition of the images.

The number of slices per scan ranged between 281 and 1033 slices, covering the thorax and part of the abdomen (in some cases) with an average slice thickness of 0.625 mm. The dataset included 20 females and 43 males. The average age was 66 years, ranging from 27 to 89 years.

The dataset was divided into two different sets. A training set of 33 cases, that was used for adjusting parameters, and a test set of 30 cases, for the validation of the developed algorithms. The only criterion employed for splitting the dataset into the two sets of training and testing was that, for a case to belong to the test set, it must include at least the celiac trunk among the visceral arteries. For the training set, this condition was not strictly necessary as it was basically used to adjust the parameters of the model developed to calculate the limits of the aortic root search interval (only the locations of both the aortic root and the brachiocephalic trunk are needed) and to set a threshold for the minimum distance between the left subclavian and the celiac trunk.

All the cases were annotated by two experts, who independently marked the positions of the aortic root and the branches. For each branch, several points inside the lumen of the branch were annotated. For the aortic root, the human experts just marked the position relative to the center of the *sinus of Valsalva*. The annotation process was performed by means of a computer provided with a touch screen, running the ITK-SNAP software and a digital stylus. Axial, coronal and sagittal projections of the original CT cases were always available simultaneously during the process. In this way, the annotation could be made in the most suitable projection. Axial projection was employed for tagging the supra-aortic branches. Celiac and superior mesenteric arteries were tagged by means of the sagittal projection. Finally, aortic root and left and right renal arteries were preferably marked on the coronal projection.

During the annotation process, different intensity values were assigned to each marked reference point. This allowed distinguishing between supra-aortic vessels (brachiocephalic, carotid and subclavian) and visceral vessels (celiac, superior mesenteric, left and right renal) in an easy way at the end of the tagging pro-

cess. Moreover, in this way, it was possible to check automatically whether the method was capable of correctly identifying the different vessels.

## 2.5 Performance Evaluation

In order to assess the accuracy of our method, we have compared the results obtained by the automatic method with those provided by each of the experts. After applying our automatic branch detection and labeling process, we must check whether they match the manual marks. Fig. 13 depicts an example of the manual marks and the detected branches. Each branch is assigned a color, in such a way that the automatically extracted branches are represented with the color corresponding to its label, and the manual marks are represented using the color corresponding to the branch they were assigned to. Therefore, if the color of the branch matches the color of the manual marks it contains, the method is working properly, as observed in Fig. 13.

To evaluate the performance of the system, recall and precision were calculated for the detected branches as follows:

$$Recall = \frac{TP}{TP + FN} \quad (11)$$

$$Precision = \frac{TP}{TP + FP} \quad (12)$$

For a given branch  $B$ ,  $TP$  (*True Positives*) is the number of branches labeled as  $B$  which are actually  $B$ .  $FP$  (*False Positives*) is the number of branches labeled as  $B$  which are not really  $B$ .  $FN$  (*False Negatives*) is the number of branches which are  $B$ , but have not been identified as such. Therefore,  $TP + FN$  is the total number of  $B$  branches and the recall (also called sensitivity or true positive rate) indicates the proportion of  $B$  branches which are properly labeled. On the other hand,  $TP + FP$  is the total number of branches labeled as  $B$  and the precision indicates the proportion of them which are actually  $B$ .

The accuracy, achieved for the detection of the aortic root was calculated by computing the distance between the reference points marked by the two experts and the locations provided by the algorithm. The centerline of the aorta was employed as the common reference for performing this computation (Fig. 13).

## 3 Results

All methods have been implemented in C++, and executed on an Intel Core i7-4790, 3.6 GHz and 16 GB RAM. The execution time (not including the time needed for reading the images from the hard disk) was less than 30 seconds. Figure 14 shows an example of the anatomical tagging procedure developed with the eight landmarks (blue points in ) that constitute the target of our method superimposed. Those landmarks, were automatically obtained from the reference points extracted from the  $CT$  volume as we have seen above. In addition, to compute the aortic arch length and its curvature a new landmark ( $AArD$ ) has been estimated. It is defined as the point on the centerline of the descending aorta which has the same z-coordinate as the  $AA$  has in the ascending aorta.

Table 1 depicts the values of recall and precision attained by our method for each branch after processing the test set. As we can see, the detection of the supra-aortic branches achieves much better results. The average value obtained for recall is 91.8%, being 98.8% for precision. Note that, since not all the CT scans include the complete set of branches, the sum of true positive and false negative cases for some of the branches (renals and mesenteric) does not match with the total number of cases. Namely, the test set contains 19 CTs with all the branches, 8 without renal arteries, and 3 without renal and mesenteric arteries. This issue does not affect the computation of the landmarks, given that the celiac artery is the only one required to obtain them.

The performance of the algorithm designed for the detection of the aortic root has been analyzed by comparing the distance between the locations calculated by the computer and the locations marked by the experts. Results are depicted in Table 2, where the difference between the locations marked by the two experts is also included. On average, the difference between the position marked by the two experts and the one detected by the computer was  $5.7 \pm 7.3$  mm, being  $5.7 \pm 8.0$  mm when compared to observer 1 and  $5.6 \pm 6.5$  mm when compared to observer 2. In addition, the average distance between the positions marked by the two observers is  $2.5 \pm 2.1$  mm, which demonstrates the high level of agreement that exists between them.

To check the validity of our method, we have calculated several commonly used anatomical distances using the calculated landmarks and we have compared the results obtained with those published in the literature. Table 3 shows the value of the diameters obtained at three different levels (landmarks *AA*, *DA* and *AaD*) separated by sex, for normal cases and also for cases with aneurysm. After [26], the value of these diameters was calculated as the mean value of the two main axes of the ellipse obtained from our segmentation process that is located at the corresponding reference point.

The lengths of the aorta for different sections were also estimated as a way to model the elongations of the descending aorta and also the shapes of the aortic arches. The values, separated by sex, which include both normal and elongated cases, are shown in Table 4. In all cases, lengths were measured on the centerline of the aorta as the distance between two of the landmarks extracted by our method. To calculate the length of the *Aortic Arch* ( $L$ ), the distance along the centerline was calculated between *AA* and *AArD*. With respect to the width of the *Aortic Arch* ( $W$ ), it was calculated as the Euclidean distance from *AA* to *AArD*.

Table 5 includes the value of several distances calculated for the examples depicted in figure 15. Aneurysms and elongations distort the normal shape of the aorta. We show that the proposed landmarks could be useful to model these different circumstances. Case *USC* – 0025 (fig15(d)) represents an elongated aorta (DA length 291 mm) with an aneurysm in the ascending section (*AA* diameter 64.2 mm) and a high curvature arch ( $W/L$  0.25). Case *USC* – 0050 represents a normal case (fig15(a)). All of the parameters seem to be normal. Case *USC* – 0068 (fig15(b)) represents an aorta with an aneurysm in the ascending section (*AA* diameter 51.7 mm). As a consequence, the shape of the arch is deformed and its curvature decreases ( $W/L$  0.81). Case *USC* – 0119 (fig15(c)) is a highly elongated aorta (DA length 396.5 mm) with an aneurysm in its descending section (*DA* diameter 38.5 mm). Finally, case *USC* – 133 (fig15(e)) represents a normal aorta, with a high-curvature arch ( $W/L$  0.31).

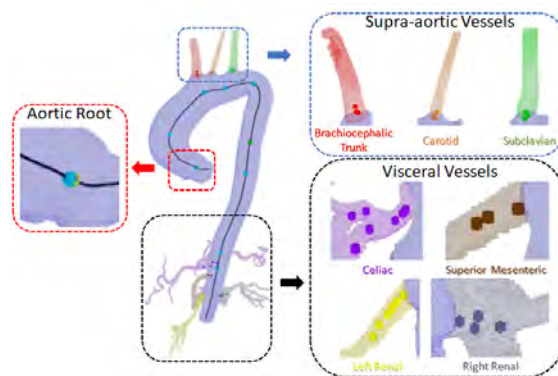


**Fig. 13** Visual representation of the correspondence assessment between the manual marks and the branches automatically labeled using the same color: ■ brachiocephalic trunk, ■ carotid, ■ subclavian, ■ celiac, ■ superior mesenteric, ■ left renal, and ■ right renal. In the aortic root we include a zoom with the detail of the manual marks of each expert in ■ and ■, and the result of the algorithm in ■ (in this case they are almost superimposed).

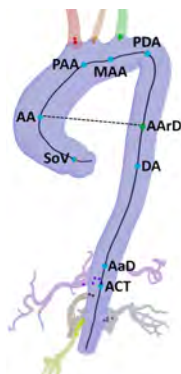


**Fig. 14** Computed landmarks and their associated labels in ■: SoV, AA, PAA, MAA, PDA, DA, AaD, and ACT (according to Fig. 1). The AA reference at the descending aorta (AArD) is also included in ■.

**Table 1** True Positives (TP), False Negatives (FN), False Positives (FP), Recall and Precision for the labeling of the supra-aortic and visceral branches.

Aortic Branch	TP	FN	FP	Recall (%)	Precision (%)
Brachiocephalic Trunk	30	0	0	100.0	100.0
Left Carotid	30	0	0	100.0	100.0
Left Subclavian	29	1	0	96.7	100.0
Celiac	26	4	0	86.7	100.0
Superior Mesenteric	23	2	2	92.0	92.0
Left Renal	16	3	0	84.2	100.0
Right Renal	14	5	0	73.7	100.0
TOTAL	168	15	2	91.8	98.8

## 4 Discussion

During the last three decades, many computer applications have been proposed in the field of medical imaging to help physicians to improve their diagnosis. Many of

**Table 2** Distance between the locations of the aortic root provided by our method and two experts.

Reference Point	Expert 1 vs Computer mm	Expert 2 vs Computer mm	Expert 1 vs Expert 2 mm
Aortic Root	$5.7 \pm 8.0$	$5.6 \pm 6.5$	$2.5 \pm 2.1$

**Table 3** Average value of the diameters of the aorta calculated at some of the landmarks in figure 14. Values separated by sex and pathology are included.

Aortic Feature	Women Normal	Aneurysm	Men Normal	Aneurysm
AA diameter (AA), mm	$29.7 \pm 4.2$	—	$34.8 \pm 4.3$	$52.3 \pm 4.2$
Proximal DA diameter (DA), mm	$21.7 \pm 2.7$	—	$24.6 \pm 3.0$	—
Distal DA diameter (AaD), mm	$20.9 \pm 2.3$	—	$24.0 \pm 3.2$	—

**Table 4** Average value of several distances related with the shape of the aorta, calculated from some of the landmarks in figure 14. Values separated by sex and pathology are included.

Aortic Feature	Women Normal	Elongation	Men Normal	Elongation
AA length (PAA - SoV), mm	$92.3 \pm 14.4$	—	$101.7 \pm 9.5$	$119.6 \pm 18.3$
DA length (PDA - ACT), mm	$212.8 \pm 14.6$	—	$220.6 \pm 15.6$	$287.4 \pm 51.3$
AArch length (AA - AArD), mm	$124.5 \pm 16.7$	—	$146.7 \pm 19.5$	$188.2 \pm 49.1$
AArch width (AA - AArD), mm	$66.2 \pm 21.1$	—	$72.9 \pm 13.9$	$90.7 \pm 29.7$
W/L (AA - AArD)	$0.50 \pm 0.13$	—	$0.50 \pm 0.08$	$48.8 \pm 12.1$

**Table 5** Diameters and distances calculated at some of the landmarks proposed in figure 14, for cases depicted in figure 15.

Aortic Feature	USC-0025	USC-0050	USC-0068	USC-0119	USC-0133
AA diameter (AA), mm	64.2	32.3	51.7	49.8	37.9
Proximal DA diameter (DA), mm	27.5	25.6	25.7	38.5	19.8
Distal DA diameter (AaD), mm	27.0	25.0	25.2	37.5	19.7
AA length (PAA - SoV), mm	150.5	94.0	102.0	126.0	106.5
DA length (PDA - ACT), mm	291.5	215.5	193.0	396.5	223.5
AArch length (AA - AArD), mm	192.0	159.0	151.5	271.0	130.5
AArch width (AA - AArD), mm	48.8	71.7	122.4	131.8	40.9
W/L (AA - AArD)	0.25	0.45	0.81	0.49	0.31

them have been related to the extraction of measures of interest from the images. Indeed, comparison of measurements obtained with past records of patients or even published reference values can be used, not only as a diagnostic mechanism, but also as a means of monitoring diseases and treatments.

Nevertheless, such information is useful only if the procedures developed for their extraction are accurate and reproducible. Achieving a high accuracy requires the existence of high quality image technologies (such would be the case with today's multi-slice CTs). However, to obtain reproducible results, it is necessary to have standard references of what is going to be measured, clear procedures of how to do it and automatic tools that eliminate the subjectivity of the human observer.

In this work, we have developed a computer tool that allows an automatic measurement of some of the distances that have traditionally been employed for diagnosis and follow-up of aortic diseases. To carry out this task, we have used several anatomical landmarks that have been defined by consensus by the experts,

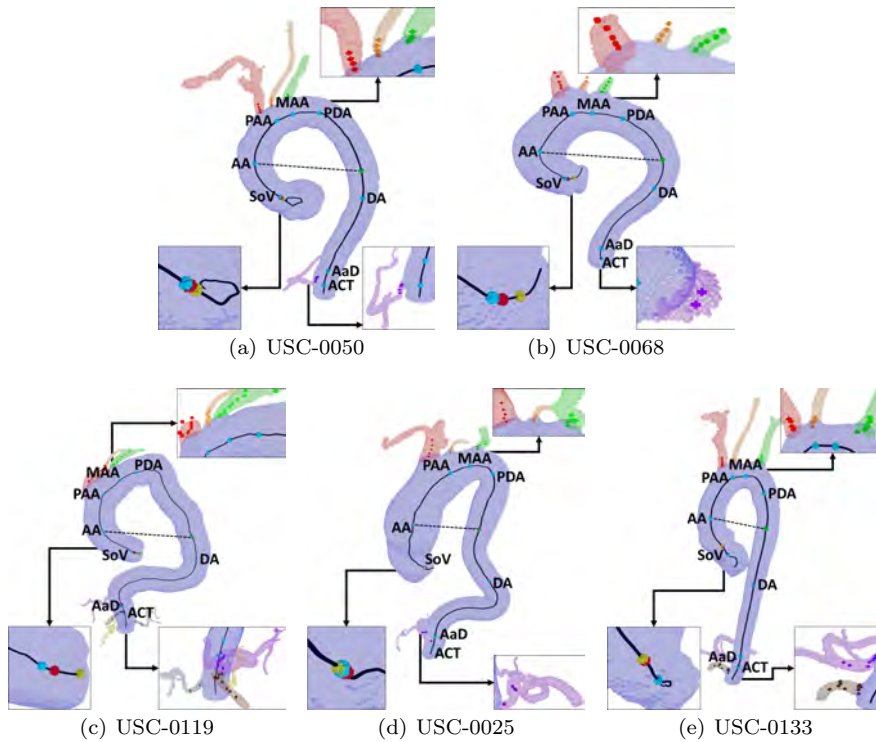


**Fig. 15** Detail of the landmarks detection for cases under different circumstances: (a) normal, (b) aneurysm, (c) elongation, (d) aneurysm and elongation, and (e) high curvature arch. We include a zoom for the main branches with the color code described in fig. 13, and for the SoV landmark with ■ expert 1, ■ expert 2, and ■ algorithm result.

based on the location of the visceral and supra-aortic branches and/or the aortic root.

As depicted in table 1, the results achieved demonstrate that the proposed algorithm is able to obtain with relatively high accuracy the main aortic branches. As we can see, the value of the recall is affected mainly by the wrong identification of some visceral arteries. A more exhaustive analysis shows that this is due to the fact that the proposed solution is highly dependent on two factors: i) the achievement of adequate growth in the expansion phase of the algorithm and ii) the correct identification of the group of visceral vessels. As for the first factor, if the expansion does not provide all the branches, the process leads to an incorrect labelling, for example when the *Celiac* artery is missing. In relation to the second factor, the process is also affected by the initialization of the threshold distance separating the supra-aortic arteries from the visceral arteries. This distance can vary considerably between individuals, depending on the size and/or degree of elongation of the aorta.

The detection of the aortic root is not an easy task for non *ECG* gated CT volumes. The state of the aortic valve (open, closed, or semi-open), is continuously changing. This fact, not only makes the shape of the root different, depending on

the instant in which the image is captured, but also makes some artifacts arise due to the movement of the heart itself.

One of the drawbacks of our method is that the detection of the root is strongly dependent on the previous location of the *Brachiocephalic Trunk* (PAA landmark, see figure 14). If this detection fails, the detection of the root is compromised. However, this rarely happens because this branch usually has a relatively large calibre and its position in the arch is prominent.

To check for the robustness of our method, we have analyzed the differences found for the location of the aortic root in two different scenarios. In the first case, the location of the *Braquiocephalic Trunk* has been automatically provided by the computer, as part of the output of the algorithm implemented for the detection of the supra-aortic branches. In the second case, the location of the *Braquiocephalic Trunk* has been provided by a human expert that marked (by hand) the position of this landmark in the reformatted volume of the *CT*. In average the accuracy achieved for the detection of the aortic root, when the location of the *Brachiocephalic Trunk* was provided by the expert (not by the computer) was similar to that achieved when the computer provided this location. The difference between both scenarios was of  $0.8 \pm 4.0$  mm. Only in 1 out of the 30 cases of our test set, the position estimated for the aortic root was affected by this issue. After analyzing this case, we have found the presence of beam hardening artifacts that could affect the performance of the aortic root detection algorithm. Nevertheless, for most of the cases, the detection of the root remains unchanged even when the location of the *Brachiocephalic Trunk* obtained by the computer does not exactly match that reported by the experts, which is usually the case.

One of the main advantages of having standard landmarks along the aorta is that it opens the possibility for comparison of measurements taken at different moments and/or different cases. Far from being something static, in many occasions, the diagnosis is based on comparing a particular case with the general behavior or on analyzing how it evolves over time. Aorta diseases are a paradigmatic example of this assertion. As Chaikof *et al* pointed out [5], a significant unmet need for aneurysm assessment is the determination of the risk of rupture. Although maximum diameter remains the most widely used and validated criterion for predicting this risk, it was based, in part, on a retrospective examination of thousands of consecutive autopsies performed at a single institution [7]. In addition, there is significant variability in aneurysm diameter reporting, and diameter measurements based on the use of axial slices have largely been replaced by the adoption of three-dimensional reformatting software. As a result, a variety of potentially more sensitive rupture risk predictors have been proposed, including the expansion velocity, wall stiffness, wall tension, and maximum aneurysm wall stress.

Even though the purpose of this paper is not the establishment of standard measures for the aorta (we do not have enough cases for that), we have compared the results achieved with our method with some of those already published in the literature in order to analyze the coherence of our methodology.

Table 3 shows the mean diameters obtained at three different levels of the thoracic aorta. Those levels are related with the landmarks we have obtained in this paper. The diameters were calculated (we only make the computation if there were at least 5 cases in our database) for normal and aneurysm cases, by gender. Reported values can be compared with those published by McComb *et al.* [20], where such measurements were obtained by hand (with the help of a computer tool) in

axial views over a data set of 322 CT cases (See table). Values of  $32.7 \pm 3.6$  (Mid-Ascending Aorta),  $24.6 \pm 2.4$  (Mid-Descending Aorta) and  $24.0 \pm 2.5$  (Diaphragmatic Hiatus) were obtained for normal women and  $34.8 \pm 3.6$  (Mid-Ascending Aorta),  $27.0 \pm 2.8$  (Mid-Descending Aorta) and  $26.4 \pm 2.6$  (Diaphragmatic Hiatus) for normal men. Minimal differences can be found, that can be justified by the fact that those values have a strong dependence on *Body Surface Area (BSA)* and age and also because, in the case of women, our database has not enough number of cases for comparisons. In fact, the values we have obtained for women are closer to those reported by Redheuil *et al.* [25], where different measurements of the aorta were manually extracted in 100 cases of *MRI* images. Values of  $30 \pm 4$  (*Mid-Ascending Aorta*),  $22 \pm 3$  (*Mid-Descending Aorta*) and  $20 \pm 2$  (*Diaphragmatic Hiatus*) were obtained for normal women. However, for normal men the diameter values are slightly lower  $31 \pm 4$  (*Mid-Ascending Aorta*),  $24 \pm 3$  (*Mid-Descending Aorta*) and  $21 \pm 3$  (*Diaphragmatic Hiatus*), demonstrating again the strong dependence of the data with the composition of the database. Finally, Kurugol *et al.* reported values for diameters of  $30.8 \pm 3.4$  mm and  $23.6 \pm 2.6$  mm for ascending and descending aorta respectively, which are also within the consensus of the different authors.

Values for aneurysm have been also reported in the literature. Diameters in the range of [50.6, 55.5] (*Mid-Ascending Aorta*) for men were reported by McComb *et al.* [20], for different *BSA* and ages. In our case, the data obtained was  $52.3 \pm 4.2$ , that perfectly fits the former interval.

Of interest in the analysis of the aorta, is the possibility of having tools to analyze lengths and geometries of the different sections. In fact, some authors have related those values with arterial stiffness, that increases with age. Table 4 depicts the values obtained by our method for lengths of different sections of the aorta. Redheuil *et al.* [25] also reports lengths for descending aorta ( $134 \pm 16$ , for women and  $143 \pm 15$  for men) and aortic arch ( $110 \pm 15$  for women and  $122 \pm 21$  for men). Results are clearly lower than those achieved by us. Thereby, it seems that the reason is that the reference point employed by these authors is the level of the *right Pulmonary Artery (rPA)*. This landmark, of common use in several studies related with the extraction of aortic features [29] is a good choice when hand extraction is employed, because, for human experts, *rPA* is easier to locate. In other cases, it is the location of the carina that is used as the reference [17] or even the axial plane at the lower level of the pulmonary artery bifurcation [30]. However, when a stand-alone computer tool is developed for tasks such as those discussed in this paper, prior detection of the *rPA* or the carina represents not only an over-effort in the design of the algorithm, but also a possible source of errors. Like [12], we have selected the landmarks proposed by Hiratzka *et al.* [13]. At this point it is interesting to see how the average value of the aortic width, reported by Redheuil *et al.* [ref] ( $66 \pm 10$  for women and  $72 \pm 11$  for men) are similar to those obtained by us. Same average value is also reported by Kurugol *et al.* [17] ( $72.8 \pm 12.3$ ). This is consistent with the fact that both the ascending and descending aorta are (in general) oriented along the longitudinal axis of the human body.

Finally, it is interesting to remark how the relationship  $W/L$  is the same for women and men and even in the case of elongations,  $W/L$  remains almost invariable. Results reported by Redheuil *et al.* for  $H/W$  ( $0.56 \pm 0.09$ ) are also the same regardless of sex. The only difference is that these authors use the height of the

aortic arch instead of its length. Once again, when this values are calculated by hand, height could have more sense, because is easier to obtain. However, for computers this limitation does not exist and the calculation of  $W/L$  is straightforward, which in fact produce a more stable value (around 0.50) for most of the cases.

## 5 Conclusions

A fully automatic method for the extraction of several standard landmarks related to the geometry of the aorta in *CTA* volumes has been proposed. To perform this task, a twofold technique has been presented, based on the extraction of the supra-aortic and visceral branches, and the aortic root detection. From both, the described landmarks are obtained. In order to asses the accuracy, a test set of 30 *CTA* cases has been used.

Related to the extraction and labeling of the branches, the algorithm successfully detects these aortic branches in most of the cases, providing a *Recall* = 95%, and a *Precision* = 100%. Regarding the aortic root, a difference of  $5.7 \pm 7.3$  mm was obtained, when the results attained by the computer were compared with the locations marked by two human experts.

To check for the validity of the results, several measurements commonly used in the diagnosis and follow-up were computed based on the landmarks extracted, and a comparison was made with the results reported in the literature. The conclusion is that values of the diameter of the *Ascending Aorta*, *Proximal Descending Aorta* and *Distal Descending Aorta*, for normal cases of men and women diameter match the results that appear in the literature. Regarding the lengths of the different sections of the aorta, although the results provided by our method were not comparable with those reported in the literature, due to the different reference landmarks employed, the results obtained were consistent with the expected values.

In conclusion, in spite of the limited number of cases employed in our study, the proposed method seems to be a useful way of modeling the geometry of the aorta. Although more cases have to be employed to prove its feasibility, a first step has been done for developing reliable and reproducible computer tools of usefulness in the diagnosis and follow-up of aortic diseases.

## Compliance with ethical standards

**Ethical approval** All procedures performed in studies involving human participants were in accordance with the ethical standards of the institutional and/or national research committee and with the 1964 Helsinki Declaration and its later amendments or comparable ethical standards. For this type of study, formal consent is not required.

## Conflict of interest

The authors declare that they have no conflict of interest.

**Acknowledgements** This research has partially been supported by the MINECO projects references TIN2016-76373-P (AEI/FEDER, UE) and MTM2016-75339-P (AEI/FEDER, UE) (Ministerio de Economía y Competitividad, Spain).

## References

1. Quantitative Imaging Biomarkers Alliance. <https://www.rsna.org/en/research/quantitative-imaging-biomarkers-alliance>. Accessed: 2019-05-30
2. Alemán-Flores, M., Santana-Cedrés, D., Alvarez, L., et al.: Segmentation of the Aorta Using Active Contours with Histogram-Based Descriptors. In: *Intravascular Imaging and Computer Assisted Stenting and Large-Scale Annotation of Biomedical Data and Expert Label Synthesis: 7th Joint International Workshop, CVII-STENT 2018 and Third International Workshop, LABELS 2018, LNCS*, vol. 11043, pp. 28–35. Springer (2018)
3. Alvarez, L., González, E., Esclarín, J., et al.: Robust Detection of Circles in the Vessel Contours and Application to Local Probability Density Estimation. In: *Intravascular Imaging and Computer Assisted Stenting and Large-Scale Annotation of Biomedical Data and Expert Label Synthesis: 6th Joint International Workshop, CVII-STENT 2017 and Second International Workshop, LABELS 2017, LNCS*, vol. 10552, pp. 3–11. Springer (2017)
4. Authors/Task Force members, Erbel, R., Aboyans, V., et al.: 2014 ESC Guidelines on the diagnosis and treatment of aortic diseases: Document covering acute and chronic aortic diseases of the thoracic and abdominal aorta of the adult. The Task Force for the Diagnosis and Treatment of Aortic Diseases of the European Society of Cardiology (ESC). *European Heart Journal* **35**(41), 2873–2926 (2014)
5. Chaikof, E.L., Dalman, R.L., Eskandari, M.K., et al.: The Society for Vascular Surgery practice guidelines on the care of patients with an abdominal aortic aneurysm. *Journal of Vascular Surgery* **67**(1), 2–77.e2 (2018)
6. Cleemann, L., Mortensen, K.H., Holm, K., et al.: Aortic Dimensions in Girls and Young Women with Turner Syndrome: A Magnetic Resonance Imaging Study. *Pediatric Cardiology* **31**(4), 497–504 (2010)
7. Darling, R.C., Messina, C., Brewster, D., et al.: Autopsy study of unoperated abdominal aortic aneurysms. The case for early resection. *Circulation* **56**(3 Suppl), 161–164 (1977)
8. Elattar, M., Wiegerinck, E., van Kesteren, F., et al.: Automatic aortic root landmark detection in CTA images for preprocedural planning of transcatheter aortic valve implantation. *The International Journal of Cardiovascular Imaging* **32**(3), 501–511 (2016)
9. Elefteriades, J.A., Farkas, E.A.: Thoracic Aortic Aneurysm: Clinically Pertinent Controversies and Uncertainties. *Journal of the American College of Cardiology* **55**(9), 841–857 (2010)
10. Entezari, P., Kino, A., Honarmand, A., et al.: Analysis of the thoracic aorta using a semi-automated post processing tool. *European Journal of Radiology* **82**(9), 1558–1564 (2013)
11. Flohr, T.G., Schaller, S., Stierstorfer, K., et al.: Multi-Detector Row CT Systems and Image-Reconstruction Techniques. *Radiology* **235**(3), 756–773 (2005)
12. Hager, A., Kaemmerer, H., Rapp-Bernhardt, U., et al.: Diameters of the thoracic aorta throughout life as measured with helical computed tomography. *The Journal of Thoracic and Cardiovascular Surgery* **123**(6), 1060–1066 (2002)
13. Hiratzka, L.F., Bakris, G.L., Beckman, J.A., et al.: 2010 ACCF / AHA / AATS / ACR / ASA / SCA / SCAI / SIR / STS / SVM Guidelines for the Diagnosis and Management of Patients With Thoracic Aortic Disease. *Journal of the American College of Cardiology* **55**(14), e27–e129 (2010)
14. Kanitsar, A., Fleischmann, D., Wegenkittl, R., et al.: CPR – Curved Planar Reformation. In: *In Visualization'02*. IEEE, pp. 37–44 (2002)
15. Kikinis, R., Pieper, S.D., Vosburgh, K.G.: 3D Slicer: A Platform for Subject-Specific Image Analysis, Visualization, and Clinical Support, pp. 277–289. Springer New York, New York, NY (2014)
16. Kitasaka, T., Egusa, T., Oda, M.: A method for nomenclature of abdominal arteries extracted from. 3D abdominal CT images based on optimizing combinations of candidate anatomical names. *International Journal of Computer Assisted Radiology and Surgery* **5**, S45–S49 (2010)

17. Kurugol, S., Come, C.E., Diaz, A.A., et al.: Automated quantitative 3D analysis of aorta size, morphology, and mural calcification distributions. *Medical Physics* **42**(9), 5467–5478 (2015)
18. Laurent, S., Cockcroft, J., Van Bortel, L., et al.: Expert consensus document on arterial stiffness: methodological issues and clinical applications. *European Heart Journal* **27**(21), 2588–2605 (2006)
19. Macía, I., Graña, M., Paloc, C.: Knowledge management in image-based analysis of blood vessel structures. *Knowledge and Information Systems* **30**(2), 457–491 (2012)
20. McComb, B.L., Munden, R.F., Duan, F., et al.: Normative reference values of thoracic aortic diameter in American College of Radiology Imaging Network (ACRIN 6654) arm of National Lung Screening Trial. *Clinical Imaging* **40**(5), 936–943 (2016)
21. Oda, M., Hoang, B.H., Kitasaka, T., et al.: Automated anatomical labeling method for abdominal arteries extracted from 3D abdominal CT images. In: *Proceedings Volume 8314, Medical Imaging 2012: Image Processing*, vol. 8314 (2012)
22. O'Rourke, M.F., Staessen, J.A., Vlachopoulos, C., et al.: Clinical applications of arterial stiffness; definitions and reference values. *American Journal of Hypertension* **15**(5), 426–444 (2002)
23. Queirós, S., Papachristidis, A., Barbosa, D., et al.: Aortic Valve Tract Segmentation From 3D-TEE Using Shape-Based B-Spline Explicit Active Surfaces. *IEEE Transactions on Medical Imaging* **35**(9), 2015–2025 (2016)
24. Rajiah, P., Schoenhagen, P.: The role of computed tomography in pre-procedural planning of cardiovascular surgery and intervention. *Insights into Imaging* **4**(5), 671–689 (2013)
25. Redheuil, A., Yu, W.C., Mousseaux, E., et al.: Age-Related Changes in Aortic Arch Geometry: Relationship With Proximal Aortic Function and Left Ventricular Mass and Remodeling. *Journal of the American College of Cardiology* **58**(12), 1262–1270 (2011)
26. Rousseau, H., Chabbert, V., Maracher, M., et al.: The Importance of Imaging Assessment Before Endovascular Repair of Thoracic Aorta. *European Journal of Vascular and Endovascular Surgery* **38**(4), 408–421 (2009)
27. Sugawara, J., Hayashi, K., Yokoi, T., et al.: Age-Associated Elongation of the Ascending Aorta in Adults. *JACC: Cardiovascular Imaging* **1**(6), 739–748 (2008)
28. Tahoces, P.G., Alvarez, L., González, E., et al.: Automatic estimation of the aortic lumen geometry by ellipse tracking. *International Journal of Computer Assisted Radiology and Surgery* **14**(2), 345–355 (2019)
29. Turkbey, E.B., Jain, A., Johnson, C., et al.: Determinants and normal values of ascending aortic diameter by age, gender, and race/ethnicity in the Multi-Ethnic Study of Atherosclerosis (MESA). *Journal of Magnetic Resonance Imaging* **39**(2), 360–368 (2014)
30. Wolak, A., Gransar, H., Thomson, L.E., et al.: Aortic Size Assessment by Noncontrast Cardiac Computed Tomography: Normal Limits by Age, Gender, and Body Surface Area. *JACC: Cardiovascular Imaging* **1**(2), 200–209 (2008)

## Authors



**Pablo G. Tahoces** has received a M.Sc. in Applied Physics in 1989 and a doctorate in Physics in 1992, both from the University of Santiago de Compostela (Spain). During the 90's he was working at the Kurt Rossmann Laboratories of the University of Chicago (USA) as Visiting Research Associate, for different periods of time. Since 2007 he is professor at the University of Santiago de Compostela. His main areas of research interest are medical imaging and computer vision.



**Daniel Santana-Cedrés** Daniel Santana-Cedrés received a M.Sc. in Computer Science, a M.Sc. in Intelligent Systems and Numerical Applications in Engineering, and a Ph.D. in Computer Science, from the University of Las Palmas de Gran Canaria, in 2011, 2013, and 2016, respectively. Since 2012, he is a member of the Imaging Technology Center (CTIM). His main research interest areas are lens distortion model estimation and medical imaging.



**Luis Alvarez** has received a M.Sc. in applied mathematics in 1985 and a Ph.D. in mathematics in 1988, both from Complutense University (Madrid, Spain). Between 1991 and 1992 he worked as postdoctoral researcher in the group led by Professor Jean-Michel Morel at CEREMADE, Université Paris IX (France). Since 2000 he is full professor at the University of Las Palmas de Gran Canaria (ULPGC). His main research interest areas are the applications of mathematical analysis to computer vision.



**Miguel Alemán-Flores** received his M.Sc. and Ph.D. degrees in Computer Science from the University of Las Palmas de Gran Canaria (Spain) in 1995 and 2002, respectively. Since 2008 he is a senior lecturer at the University of Las Palmas de Gran Canaria. His main research areas are image processing, computer vision and medical imaging.



**Agustín Trujillo** has received a M.Sc. Degree and a Ph.D. in Computer Science from the University of Las Palmas de Gran Canaria (Spain). Since 2012 he is professor at the University of Las Palmas de Gran Canaria. His main research interest areas are image analysis (specifically in image feature extraction and 2D and 3D medical imaging), and computer graphics (terrain visualization and virtual globe development for mobile devices).



**Carmelo Cuenca** has received a M.Sc. Degree in Physical Science from Complutense University (Madrid, Spain) and a Ph.D. in Computer Science from the University of Las Palmas de Gran Canaria (Spain). Since 1998 he is senior lecturer at the University of Las Palmas de Gran Canaria. His main research interest areas has been real-time image processing for professional applications and high performance solutions including topics like multiprocessors, distributed systems, heterogeneous computing and cloud computing.



**Jose M. Carreira** is Medical Doctor since 1983 and received the Ph.D. degree in 1991 from the University of Santiago de Compostela (Spain). Between 1993 and 1998 he worked as vascular and interventional radiologist with Prof. Manuel Maynar at the University Hospital of Las Palmas de Gran Canaria (Spain). Since 1998 he is a professor at the University of Santiago de Compostela and his main research interests are focused on the peripheral vascular imaging analysis and the vascular intervention.